Available online at www.sciencedirect.com
ScienceDirect
Thermochimica Acta 450 (2006) 38–41
thermochimica acta
www.elsevier.com/locate/tca

Single crystal growth of $Bi_{1-x}Sr_xMnO_3$—Thermodynamics and experiment

D. Sedmidubský [a,*], M. Nevřiva [a], J. Leitner [b], A. Strejc [a]

[a] *Department of Inorganic Chemistry, Institute of Chemical Technology, Technická 5, 166 28 Prague, Czech Republic*
[b] *Department of Solid State Engineering, Institute of Chemical Technology, Technická 5, 166 28 Prague, Czech Republic*

Available online 28 July 2006

Abstract

The primary crystallization field of a perovskite solid solution $Bi_{1-x}Sr_xMnO_{3-\delta}$ was delimited by calculating the respective phase equilibria in the quaternary Bi–Sr–Mn–O system. The calculations are based on the recent assessment involving all three ternary subsystems, a quaternary liquid approximated as a mixture of Mn, MnO, Mn_2O_3, SrO and Bi_2O_3 species with binary Redlich–Kister coefficients and the perovskite phase described in terms of a point defect model allowing Sr^{2+} for Bi^{3+} substitution, oxygen vacancy formation and the related Mn^{3+}/Mn^{4+} mixing on Mn-sublattice. The crystallization path and the composition of the crystallized solid solution are compared with single crystal growth experiments performed by self-flux method from a Bi-rich melt. The crystallization path obtained for a selected feed composition for which the largest and high quality single crystal have been grown, turns out to end very close to the global eutectic point.

Keywords: Bi–Sr–Mn–O system; Thermodynamic modeling; Phase diagrams; Crystal growth

1. Introduction

The Bi-based perovskite manganites, $Bi_{1-x}Sr_xMnO_3$, have been recently extensively investigated due to a metal-insulator transition provoked by Mn^{3+}/Mn^{4+} charge ordering that has been observed at exceptionally high temperatures. The charge ordering temperature reaches a maximum value $T_{CO} \sim 610$ K for the ultimate composition $x = 0.3$ [1], which represents a Bi–Sr miscibility limit on the Bi-rich side. Whereas this single-phase borderline reveals only a minute dependence on temperature and oxygen activity, the solid solubility on the Sr-rich side has been found to extend markedly from $x \sim 0.6$–0.7 below 1000 °C up to $x = 1$ above ~1500 °C in air atmosphere. The stabilization of the normal perovskite phase over the hexagonal perovskite α-$SrMnO_3$ is apparently due to a substantial loss of oxygen and is thus favored at elevated temperatures and/or reduced partial pressures of oxygen. As the oxygen vacancies tend to order, the resulting structure is an orthorhobically distorted perovskite with an utmost stoichiometry $SrMnO_{2.5}$ [2]. However, the latter composition has only been stabilized in Ar/H_2 atmosphere at ~1500 °C, while in air or at moderately reduced oxygen activity a formation of another end member, $SrMnO_{2.6}$, has been identified [3]. On the Bi-rich side, the $Bi_{1-x}Sr_xMnO_3$ phase coexists with Mn_3O_4 and $BiMn_2O_5$ at normal conditions and its stabilization towards $BiMnO_3$, a heavily distorted perovskite with *C2* symmetry, can only be achieved by applying high pressure (6 GPa, 700 °C) [4].

A detailed structural analysis revealing the nature of charge and orbital ordering phenomena in $Bi_{1-x}Sr_xMnO_3$ and particularly the role of Bi^{3+} lone pair in it, requires the availability of high quality single crystals. These have been recently grown by self-flux method from Bi-rich melt [5]. A batch of a typical nominal composition $x_{Bi} \sim 0.75$–0.82 and $x_{Mn} \sim 0.12$–0.15 was slowly cooled (1 K/h) from 1100 to 1250 °C down to 850 °C and the single crystals (cubes up to 10 mm) were recovered by quickly drawing off the remaining melt. The diffraction experiments performed on the prepared crystals revealed an ordering into Mn^{3+}–Mn^{3+}–Mn^{4+}–Mn^{4+} double stripes and the susceptibility measurements indicated a formation of Zener pairs Mn^{3+}–Mn^{4+} with strong double exchange ferromagnetic interaction. An antiferromagnetic ordering of pseudo CE-type was also found to occur below $T_N \sim 150$ K for $x = 0.5$ [6].

More recently we accomplished a thermodynamic assessment of the Bi–Sr–Mn–O system and calculated some representative isothermal and pseudobinary sections for fixed oxygen activity with a focus on the phase stability of $Bi_{1-x}Sr_xMnO_3$ and its coexistence with other phases including the high temperature liquid [7]. Let us note that we did not take use of any

* Corresponding author. Fax: +420 2 24311010.
E-mail address: sedmidub@vscht.cz (D. Sedmidubský).

0040-6031/$ – see front matter © 2006 Elsevier B.V. All rights reserved.
doi:10.1016/j.tca.2006.07.015

experimental input from the single crystal growth when assessing the thermodynamic data of the respective phases. In this paper, we employ the existing thermodynamic model to describe the crystal growth process of $Bi_{1-x}Sr_xMnO_3$ perovskite by equilibrium calculations and to compare the theoretical results with the experiment.

2. Thermodynamic model and calculation

The oxygen rich part of the quaternary system Bi–Sr–Mn–O contains several stoichiometric mixed oxide phases belonging to the respective ternary subsystems Sr–Mn–O, Bi–Sr–O and Bi–Mn–O. The only quaternary phases considered in this study are the perovskite solid solution $Bi_{1-x}Sr_xMnO_{3-\delta}$ and the high temperature liquid. All stoichiometric phases, which are, apart from the constituent unary oxides, $BiMn_2O_5$, $Bi_{12}MnO_{20}$, Sr_2MnO_4, $Sr_3Mn_2O_7$, $Sr_7Mn_4O_{15}$, $Sr_4Mn_3O_{10}$, Bi_2SrO_4, $Bi_2Sr_2O_5$, $Bi_2Sr_3O_6$ and $Bi_2Sr_6O_{11}$, were described by their Gibbs energy functions constructed from the enthalpies of formation and entropies at $T_{ref} = 298.15$ K, and the temperature dependencies of heat capacity [7].

Moreover, in the Sr–Mn–O ternary $SrMn_3O_{6-z}$, α-$SrMnO_{3-\delta}$ and the end member of $Bi_{1-x}Sr_xMnO_{3-\delta}$, β-$SrMnO_{3-\delta}$, exhibit an apparent oxygen deficiency. This fact was taken into account by considering, respectively, the mixtures of $SrMn_3O_6$–$SrMn_3O_{5.5}$ and α,β-$SrMnO_3$–$SrMnO_{2.5}$ with excess Gibbs energy terms resulting from the ideal mixing entropies of the corresponding sublattice models. The model for β-$SrMnO_{3-\delta}$ was further extended to $Bi_{1-x}Sr_xMnO_{3-\delta}$ assuming the third hypothetical perovskite end member $BiMnO_3$. This turned out to be an adequate approximation, since the structure tends to be oxygen deficient only on the Sr-rich part, while the Bi-rich compositions reveal an ideal oxygen stoichiometry. As with the previous non-stoichiometric solid phases the thermodynamic treatment of $Bi_{1-x}Sr_xMnO_{3-\delta}$ was essentially based on a sublattice formalism, but the ideal mixing terms from the respective sublattices were rewritten to separate the ideal mixing entropy term related to the end members given above from the remaining part treated as an excess Gibbs energy. Moreover, an additoinal non-ideal interaction term between $BiMnO_3$ and β-$SrMnO_3$ was considered.

The non-stoichiometric phases from the Bi–Sr–O ternary system, namely β, γ and δ solid solutions, were described by compound energy formalism taken from Hallstedt et al. [8]. The only modification concerns the δ phase, for which a slightly different entropy term in the reciprocal relation $\Delta G_r = 11900 + 120T$ was applied in order to retain the consistency with our model for liquid phase. The thermodynamic behavior of the high temperature quaternary liquid was modeled as a solution of Mn, MnO, Mn_2O_3, SrO and Bi_2O_3 liquid species with binary temperature dependent Redlich–Kister coefficients.

The formulas for the pertinent models and all used thermodynamic data are given in our latest paper [7] including the applied assessment approach. However, unlike the latter work, we transferred all data and thermodynamic models from our Chemeq Gibbs energy minimizer into FactSage platform and performed all current calculations by means of FactSage [9]. As the growing experiments were carried out in normal air atmosphere, all phase diagrams were also calculated for a fixed partial pressure of oxygen ($p_{O_2} = 0.21$). However, the thermodynamic models of the relevant phases are constructed to allow for the variation of oxygen stoichiometry so that the oxygen potential can be in principle fixed to any arbitrary value (except for very low partial pressures for which metal phases are formed).

3. Experimental part

Since all known manganites melt incongruently, the application of common "own-melt" methods for single crystal growth are excluded. Hence, the single crystals of the Bi-based manganites were grown using the conventional flux method with an excess of Bi_2O_3 used as flux. The contamination of grown crystals by the flux components was thus minimized. Each experimental run started by the determination of the saturation temperature using high temperature microscopy chamber mounted in a microscope with a reflected-light observation option. The melts were prepared by thoroughly mixing the analyzed powdered starting materials ($SrMnO_3$, MnO_2 and Bi_2O_3) and putting them into 25 cm^3 platinum crucibles. The crucible was then placed into a muffle furnace. The temperature was raised slowly up to ~50 K above the liquidus temperature and maintained for a period of 12 h. After a soaking period the temperature was decreased at a rate of 1 K/h down to 850 °C. The crystals were then separated by pouring out the melt on a porous ceramic block in the furnace which was then switched off and allowed to cool rapidly to room temperature. Experimental conditions and nominal compositions of the melts used for crystal growth are in detail described in [5].

4. Results and discussion

The high temperature microscopy tests revealed the liquidus temperatures ranging from 1310 to 1480 K depending on the overall composition. In general, the experimental liquidus temperatures are by 60–100 K higher than the calculated ones. Let us note that the sample holder was not equipped with any direct temperature sensor and the temperature calibration was only done by correlating the input heating power with the melting points of several inorganic substances. Although the calibration was fairly reproducible (±10 K), a systematic error in determining the liquidus temperature cannot be excluded. In order to examine more in detail the solidification process and single crystal growth of the perovskite phase, we selected a single representative composition ($x_{Bi} = 0.82$, $x_{Mn} = 0.12$), from which high quality single crystals (homogeneous, 5–10 mm, low concentration of cracks and inclusions) have been grown. In this particular case, the measured liquidus temperature was $T_L = 1323$ K, while the calculation yielded $T_L = 1260$ K.

The phase relations at temperatures 1125, 1373 and 1500 K in air atmosphere and at 1373 K for $p_{O_2} = 10^{-4}$ have been reported in our previous paper [7]. We recalculated these phase diagrams and found no differences brought about by the conversion from Chemeq to FactSage. Let us recall that at high temperatures the stability field of the perovskite solid solution

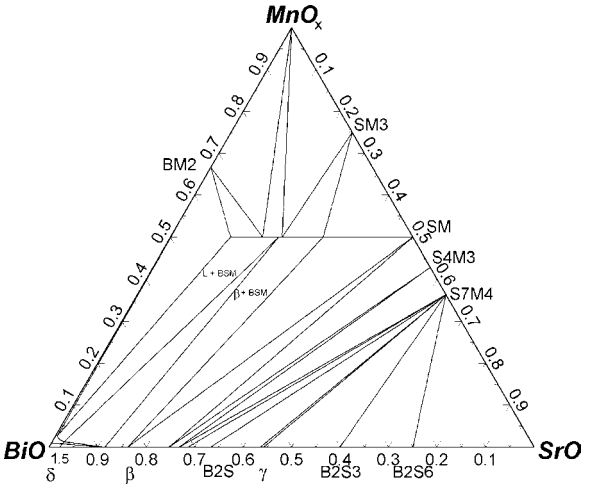

Fig. 1. Isothermal ($T = 1085$ K) and isoactivity ($p_{O_2} = 0.21$) section of the Bi–Sr–Mn–O phase diagram. The phase symbols are shortcuts formed from first letters of the constituent oxides.

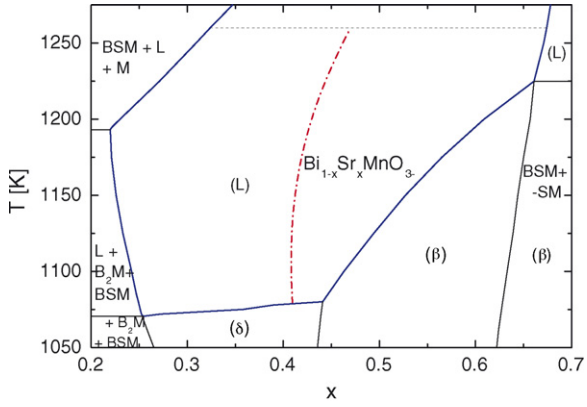

Fig. 2. Stability field of $Bi_{1-x}Sr_xMnO_{3-\delta}$ and the neighboring 3-phase regions. Symbols in parantheses L, β, δ stand for the coexisting phases (two-phase fields) in the Bi, Sr-rich part of the phase diagram. (- · - · - ·) Equilibrium composition of a crystal grown from the nominal batch composition $x_{Bi} = 0.82$, $x_{Sr} = 0.06$ cooled from the liquidus temperature (1260 K, - - -) down to the solidus temperature (1079 K).

$Bi_{1-x}Sr_xMnO_{3-\delta}$ is delimited by liquid-$BiMn_2O_5$-perovskite three-phase region at the Bi-rich side ($BiMn_2O_5$ being replaced by Mn_3O_4 above 1193 K) and by perovskite-α-$SrMnO_{3-\delta}$ two-phase field at Sr-rich side. At 1508 K, the liquid-Mn_3O_4-perovskite invariant point crosses the $x_{Mn} = 0.5$ pseudobinary line and $Bi_{1-x}Sr_xMnO_{3-\delta}$ starts to coexist with a pure liquid on Bi-rich side. Furthermore, a peculiar feature occurs in air atmosphere at 1558 K—according to our calculations the perovskite phase disappears completely at the expense of α-$SrMnO_{3-\delta}$ and is reestablished at 1618 K extending, with increasing temperature, towards β-$SrMnO_{3-\delta}$. With the exception of this interval, which can be even eliminated by reducing p_{O_2}, the perovskite forms a continuous two-phase coexistence field with the liquid phase ranging from the melting point of β-$SrMnO_{3-\delta}$ (2013 K in air) down to the global eutectic point. The quaternary eutectic ($T_E = 1070.5$ K, $x_{Bi} = 0.976$, $x_{Bi} = 0.021$, in air) is situated very close to the eutectic point of the Bi_2O_3–MnO_x system ($T_E = 1076$ K, $x_{Bi} = 0.983$) and just below the isothermal section (1085 K) depicted in Fig. 1.

As seen from the diagram in Fig. 1, $Bi_{1-x}Sr_xMnO_{3-\delta}$ forms two-phase fields with $BiMn_2O_5$, Mn_3O_4 and $SrMn_3O_{6-z}$ in the Mn-rich part and with liquid and β-phase on the Bi, Sr-rich part. The partition of the perovskite stability field into two parts (L) and (β) representing, respectively, the coexistence with liquid and β-phase can be even more clearly viewed from Fig. 2. In a narrow temperature between $T = 1080$ K, when an equilibrium with δ-phase is established, and T_E, when the liquid disappears, the field is even splitted into three parts. Shown in Fig. 2 is also the evolution of composition x of a perovskite crystal grown from our sample batch composition upon cooling from liquidus down to a complete solidification. During the entire cooling the batch composition is found in the perovskite primary crystallization field (see also Fig. 3) until a three-phase field δ–L-perovskite is reached at $T = 1079$ K. However, just 1 K below the liquid solidifies completely. Note that this concentration curve represents an equilibrium case which can only be achieved provided a sufficiently fast diffusion in the crystal. Nevertheless, as the Bi/Sr ratio in the perovskite varies only slightly along the crystallization path, we are likely not very far from this ideal case. It is also worth to mention that the final composition $x = 0.41$ (corresponding to both the solidus point and the temperature ~1123 K at which the melt was drawn off) is in fairly good agreement with $x = 0.46$ as obtained by electron microprobe.

Last, the crystallization path itself (composition of the liquid being in equilibrium with the crystal) is plotted in Fig. 3 along with the primary crystallization field represented as contours of the liquidus lines at selected temperatures and as the evolution of invariant end points from the particular liquidus temperature 1260 K down to the eutectic point. A draft of phase relations at $T = 1260$ K is also given in the diagram.

The single crystals of $Bi_{1-x}Sr_xMnO_{3-\delta}$ prepared so far exhibited only a limited composition range $x \sim 0.45$–0.50. This

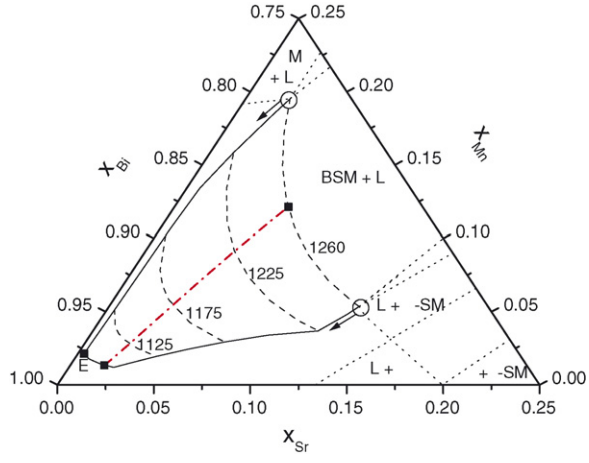

Fig. 3. Primary crysallization field of $Bi_{1-x}Sr_xMnO_{3-\delta}$ with contours (- - -) corresponding to isothemal liquidus lines. (- · - · - ·) Crystallization path (liquid composition) for the nominal batch composition $x_{Bi} = 0.82$, $x_{Mn} = 0.12$ cooled from the liquidus temperature (1260 K, - - -) down to the solidus temperature (1079 K). (. . .) Phase relations in the isothermal section corresponding to liquidus temperature 1260 K. ■– start and end composition of the crystallized melt and the global eutectic point E at $T = 1070.5$ K.

study brings a guideline for growth experiments providing crystals with much more variable bismuth composition. To get the Sr-rich composition one would need, apart from varying the initial batch composition towards Sr, to interrupt the cooling and separate the crystals from melt at higher temperatures. The simultaneous crystallization of the β-phase would be thereby avoided. The preparation of more Bi-rich crystals is indeed confined to the Bi–Sr miscibility limit. Nevertheless, the crystals containing as low as $x = 0.25$ of Sr could be theoretically obtained by properly adjusting the melt composition and the cooling interval.

5. Conclusions

The thermodynamic study of the Bi–Sr–Mn–O system reported in this paper is primarily based on the assessment of the individual ternary systems. The quaternary liquid is approximated in terms of only binary interactions between the respective liquid oxide species and even the model of the $Bi_{1-x}Sr_xMnO_{3-\delta}$ perovskite mainly relies on the thermodynamic description of the end members β-$SrMnO_3$, β-$SrMnO_{2.5}$ and the hypothetical $BiMnO_3$ with a single interaction serving only as a fine-tuning parameter. Despite the minor experimental input from the quaternary system, the phase relations determined independently by experiment, in particular the perovskite stability range and its equilibrium with liquid phase as resulted from single crystal growth and subsidiary tests, are quite well reproduced. The present thermodynamic model can thus be employed as a theoretical tool for designing controlled growth experiments to get single crystals exhibiting the requisite characteristics.

Acknowledgements

This work was supported by the Czech Science Foundation, Grant No. 203/03/0924 and the Ministry of Education of the Czech Republic (Grant No. 6046137302).

References

[1] C. Frontera, J.L. García-Munoz, C. Ritter, L. Manosa, X.G. Capdevila, A. Calleja, Solid State Commun. 125 (2003) 277.
[2] V. Caignaert, N. Nguyen, M. Hervieu, B. Raveau, Mater. Res. Bull. 20 (1985) 497.
[3] D. Sedmidubský, A. Strejc, M. Nevřiva, J. Leitner, C. Martin, Solid State Phenom. 90–91 (2003) 427.
[4] T. Atou, H. Chiba, K. Ohoyama, Y. Yamaguchi, Y. Syono, J. Solid State Chem. 145 (1999) 639.
[5] M. Nevřiva, P. Beran, D. Sedmidubský, A. Strejc, J. Hejtmánek, C. Martin, J. Perez, S. Malo, B. Raveau, Solid State Phenom. 90–91 (2003) 371.
[6] J. Hejtmánek, K. Knížek, Z. Jirák, M. Hervieu, C. Martin, M. Nevřiva, P. Beran, J. Appl. Phys. 93 (2003) 7370.
[7] D. Sedmidubský, J. Leitner, O. Beneš, Calphad 30 (2006) 179.
[8] B. Hallstedt, D. Risold, L.J. Gauckler, J. Am. Ceram. Soc. 80 (1997) 1085.
[9] FactSage™, Version 5.4.1, © Thermfact Ltd. & GTT-Technologies mbH, www.factsage.com.